Received: 31 May 2023 | Revised: 4 July 2023 | Accepted: 23 July 2023

DOI: 10.1111/exd.14902

CONCISE COMMUNICATION

Experimental Dermatology WILEY

Far-UVC- and UVB-induced DNA damage depending on skin type

Loris Busch[1,2] | Marius Kröger[1] | Daniela F. Zamudio Díaz[1,3] | Johannes Schleusener[1] | Silke B. Lohan[1] | Jackie Ma[4] | Christian Witzel[5] | Cornelia M. Keck[2] | Martina C. Meinke[1]

[1]Department of Dermatology, Venereology and Allergology, Center of Experimental and Applied Cutaneous Physiology, Charité – Universitätsmedizin Berlin, Corporate Member of Freie Universität Berlin and Humboldt-Universität zu Berlin, Berlin, Germany

[2]Department of Pharmaceutics and Biopharmaceutics, Philipps-Universität Marburg, Marburg, Germany

[3]Technische Universität Berlin, Institute of Food Technology and Food Chemistry, Berlin, Germany

[4]Department of Artificial Intelligence, Fraunhofer Heinrich Hertz Institute, Berlin, Germany

[5]Division of Plastic and Reconstructive Surgery, Department of Surgery, Charité – Universitätsmedizin Berlin, Corporate Member of Freie Universität Berlin and Humboldt-Universität zu Berlin, Berlin, Germany

Correspondence
Loris Busch, Department of Dermatology, Venereology and Allergology, Center of Experimental and Applied Cutaneous Physiology, Charité—Universitätsmedizin Berlin, Freie Universität Berlin and Humboldt-Universität zu Berlin, Charitéplatz 1, 10117 Berlin, Germany.
Email: loris.busch@charite.de

Funding information
Bundesministerium für Bildung und Forschung, Grant/Award Number: VIMRE-03ZZ0146B and CORSA-03COV10C

Abstract

Far-UVC radiation sources of wavelengths 222 nm and 233 nm represent an interesting potential alternative for the antiseptic treatment of the skin due to their high skin compatibility. Nevertheless, no studies on far-UVC-induced DNA damage in different skin types have been published to date, which this study aims for. After irradiating the skin with far-UVC of the wavelengths 222 and 233 nm as well as broadband UVB, the tissue was screened for cyclobutane pyrimidine dimer-positive (CPD^+) cells using immunohistochemistry. The epidermal DNA damage was lower in dark skin types than in fair skin types after irradiation at 233 nm. Contrary to this, irradiation at 222 nm caused no skin type-dependent differences, which can be attributed to the decreased penetration depth of radiation. UVB showed the relatively strongest differences between light and dark skin types when using a suberythemal dose of 3 mJ/cm^2. As melanin is known for its photoprotective effect, we evaluated the ratio of melanin content in the stratum basale and stratum granulosum in samples of different skin types using two-photon excited fluorescence lifetime imaging (TPE-FLIM) finding a higher ratio up to skin type IV–V. As far-UVC is known to penetrate only into the upper layers of the viable skin, the aforementioned melanin ratio could explain the less pronounced differences between skin types after irradiation with far-UVC compared to UVB.

KEYWORDS
cyclobutane pyrimidine dimers, DNA damage, far-UVC, melanin, photo-protection

Loris Busch and Marius Kröger contributed equally to this work.

1 | BACKGROUND

Following the increased interests in room disinfection and skin antisepsis during the COVID-19 pandemic, studies have been conducted to prove the bactericidal[1–6] and virucidal[7–9] potential of far-UVC radiation (100–240 nm). UVC radiation (100–280 nm) is known to be absorbed by nucleic acids and proteins. As a result of photo-induced pyrimidine dimerisation, DNA lesions including cyclobutane pyrimidine dimers (CPDs) and pyrimidine (6-4) pyrimidone photoproducts (6-4PPs) are formed in microorganisms[10] and epidermal cells[11] with a generally higher abundance of CPDs.[2,12] Thus, far-UVC radiation can potentially be used for disinfection purposes, for example, in hospitals, but also has to be assessed regarding its potential risks for human health. Interestingly, it was shown that far-UVC radiation of 222 and 233 nm produces less DNA damage in skin than UVC radiation of 254 nm, which is often used for the disinfection of surfaces or water, but still shows bactericidal effects.[2,3,6] However, to date, only studies on skin type-dependent protection against DNA damage after irradiation with simulated solar UV radiation have been performed on skin,[13–17] but no investigations have yet been conducted on skin type-dependent protection against far-UVC.

In the present study, we correlated measurements of the absorptiometrically measured melanin index (MI) and histological assessments of irradiated skin thin sections with the two-photon excited fluorescence lifetime imaging (TPE-FLIM) visualisation of the distribution of melanin in the epidermis of non-irradiated skin thin sections and a semantic machine learning model revealing the distribution of DNA damage in the epidermis.

1.1 | Questions addressed

Does the radiation-related formation and localisation of DNA damage in different skin types depend on the applied wavelength of UV light?

1.2 | Experimental design

See Data S1.

2 | RESULTS

For the visualisation of melanin distribution in human skin, cryohistological thin sections of $n = 13$ resected skin samples of Fitzpatrick's skin type I–VI were evaluated. Sections were imaged using TPE-FLIM.[18,19] The melanin distribution in the epidermis can be assessed using TPE-FLIM via the mean lifetime τ_m, where melanin is a significant contributor of very short fluorescence lifetimes. The mean fluorescence lifetime τ_m is defined as the weighted average of the lifetime components τ_1 *(short lifetime component)* and τ_2 (long lifetime component) in each pixel of the image and their respective amplitudes a_1 and a_2 *described as*,

$$\tau_m = \frac{a_1\tau_1 + a_2\tau_2}{a_1 + a_2} \quad (1)$$

τ_m was measured along the stratum basale (SB) and along the upper stratum granulosum (SG). From this, the ratio of τ_m of SG/τ_m of SB was calculated to represent the epidermal melanin gradient.

The mean lifetime τ_m measured in the skin is significantly influenced by the strikingly short lifetime of melanin.[20,21] As a result, short lifetimes in the skin sections correlate with a high melanin concentration in the skin. As a first step, the MI of the skin samples was determined in order to obtain a quantifiable indication of the general melanin content of the respective skin type. The mean lifetime of the SB was then correlated with the previously measured MI of the skin. Figure 1A shows a corresponding exponentially decreasing fluorescence lifetime with increasing amount of melanin. The dependence of fluorescence lifetime and MI could be fitted using an exponential decay function with $a = 183{,}11$; $b = 33.54$ and an adjusted $R^2 = 0.71$ described as,

$$\mathrm{FIT}_{\tau_{mSB}} = e^{\frac{a}{MI+b}} \quad (2)$$

Interestingly, the distinction between relatively dark skin types is more difficult, as the short lifetime of melanin approximates the detection limit of time-correlated single-photon counting (instrument response function) between 80 and 100 ps.[22] Thus, the curve flattens out towards higher MI values because of the high sensitivity of TPE-FLIM to the high fluorescence of melanin. As presented in Figure 1B, the mean lifetime in the SG of light skin types decreases comparatively less as compared to the SB with an inverse linear correlation with an adjusted $R^2 = 0.93$, intercept $n = 1111.11 \pm 10.04$ and slope $m = -0.89 \pm 0.02$ described as,

$$\mathrm{FIT}_{\tau_{mSG}} = n + (m\,MI) \quad (3)$$

Resulting from this, the ratio of the mean lifetime in the SG and SB, representing the melanin gradient of the skin from basal to corneal, increases with the MI, indicating a stronger melanin gradient in darker skins (Figure 1C). Interestingly, the skin with a MI of 998 has a lower ratio of the mean lifetime in the SG and SB, presumably due to a saturation of basal melanin, where only the increase of melanin in SG can be detected. However, this effect should be further investigated in future studies to provide an improved representation of the relationship between the two variables.

Representative histological sections (CPD^+ staining and unstained TPE-FLIM images) are depicted in Figure 1D to show the melanin content and distribution in the different skin types.

In parallel, we irradiated the human skin resected at least 24 h after surgery with 10% of a minimum erythema dose (MED) (3 mJ/cm^2) with a broadband UVB lamp, with a 233 nm LED and a 222 nm excimer lamp with a microbiocidal dose (40 mJ/cm^2)[2,23] and evaluated the abundance of CPD-positive (CPD^+) cells immunohistologically.[1,2]

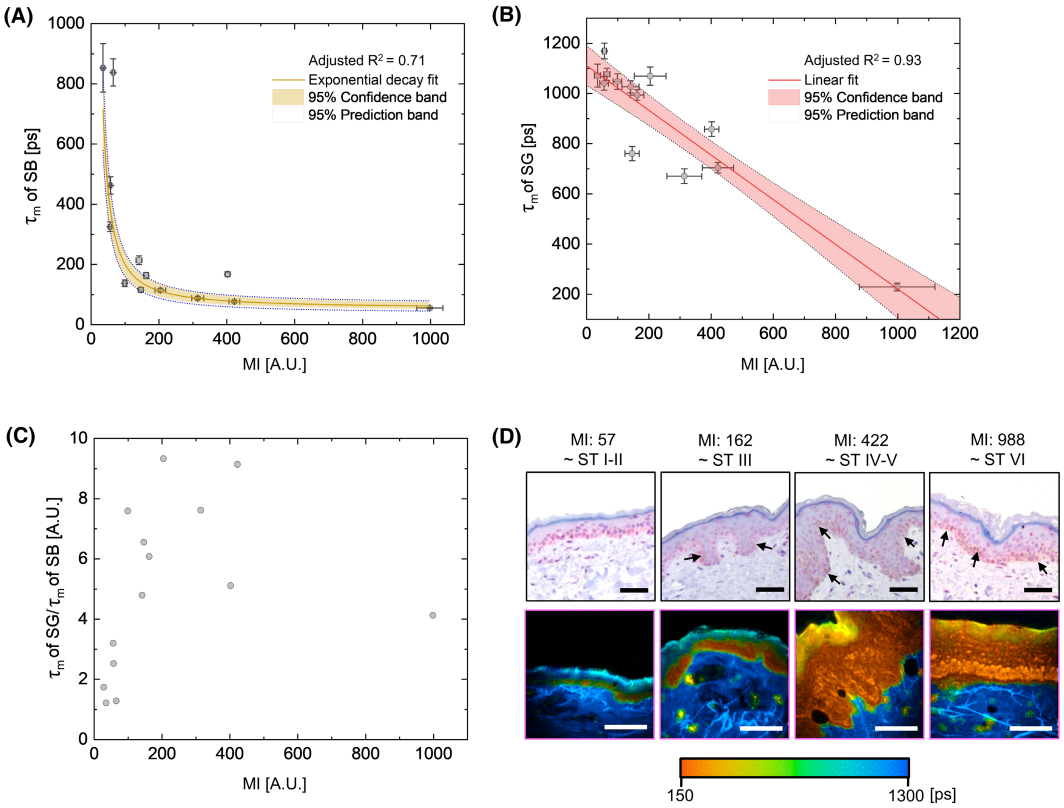

FIGURE 1 (A) Inverse correlation of the mean fluorescence lifetime τ_m of the stratum basale (SB) and melanin index (MI) fitted by an exponential decay function (golden line) with an adjusted R^2 of 0.71 including the 95% confidence band (golden area) as well as 95% prediction band (dotted line). (B) Correlation of the mean fluorescence lifetime τ_m of the stratum granulosum (SG) and MI fitted by an inverse linear function (red line) with an adjusted R^2 of 0.93 including the 95% confidence band (red area) as well as 95% prediction band (dotted line). (C) Representation of the ratio of mean fluorescence lifetime τ_m of the SG and SB in dependence of the MI. Data of $n = 13$ ex vivo skin samples. (D) Illustration of histological sections with immunohistological CPD^+ staining representative for the different skin types (upper row, arrows were used to mark the basal melanin) as well as unstained cryohistological TPE-FLIM images with representation of the mean fluorescence lifetime τ_m visualised in false colours for lifetimes between 150 ps (orange) and 1300 ps (blue) (lower row). Scale bars are corresponding to 50 µm. The authors refer to the online version of the article for colour representation.

The individual doses were chosen based on a publication by Zwicker et al.,[2] who demonstrated that after irradiation with UVB at 10% of a MED (Fitzpatrick skin type II), CPD^+ cells are highly abundant in light skin types. To avoid a possible saturation effect on CPD^+ abundance after irradiation with UVB in light skin types and to ensure comparability between light and dark skin types, we decided not to increase the dose and to compare it with microbiocidal doses of far-UVC. The far-UVC doses applied (40 mJ/cm^2) were also within the sub-erythemal range, as shown in recent publications by Eadie et al.[24] and Zamudio Díaz et al.[12]

Furthermore, the area score of CPD^+ cells representative for the distribution of DNA damage in the epidermis was calculated using a semantic machine learning model as previously described elsewhere.[25] The area score S_{area} was calculated as the ratio of the area of the epidermis and the area of semantic segmentation maps of damaged cells in the epidermis.

It is noticeable that after irradiation with 10% MED UVB, skin type I–III showed an increased abundance of CPD^+ cells by a factor of two as compared to skin type IV–VI (Figure 2A, $p < 0.05$). This difference is also evident for 233 nm 40 mJ/cm^2, while no differences were observed for 222 nm 40 mJ/cm^2. This could be related to the fact that the penetration depth of UVB is known to be higher than that of far-UVC.[2,12,26] Furthermore, it is known that the penetration depth of 233 nm is slightly increased compared to 222 nm.[2] Dark skin types have a higher melanin content than light skin types, especially in the SB, while the differences in the SG between skin types are smaller as already presented. As UVB penetrates the entire epidermis, skin types IV–VI show increased protection. Due to the fact that 222 nm penetrates the skin only superficially and the difference in melanin content between light and dark skin types is comparatively smaller in this area, the abundance of CPD^+ cells in the skin showed no significant differences between the skin types.

Using the area score, which is suitable for mapping the depth of damage, the differences in damage for UVB and 233 nm were less pronounced between light and dark skin types (Figure 2B). However, we found (partially) intact basal layers in two of the four dark skin sections evaluated after irradiation with UVB (Example Figure 2C), while the other two skin sections showed evenly distributed lesional areas. On the other hand, the light skin counter parts showed CPD^+ cells in the whole epidermis. This might be

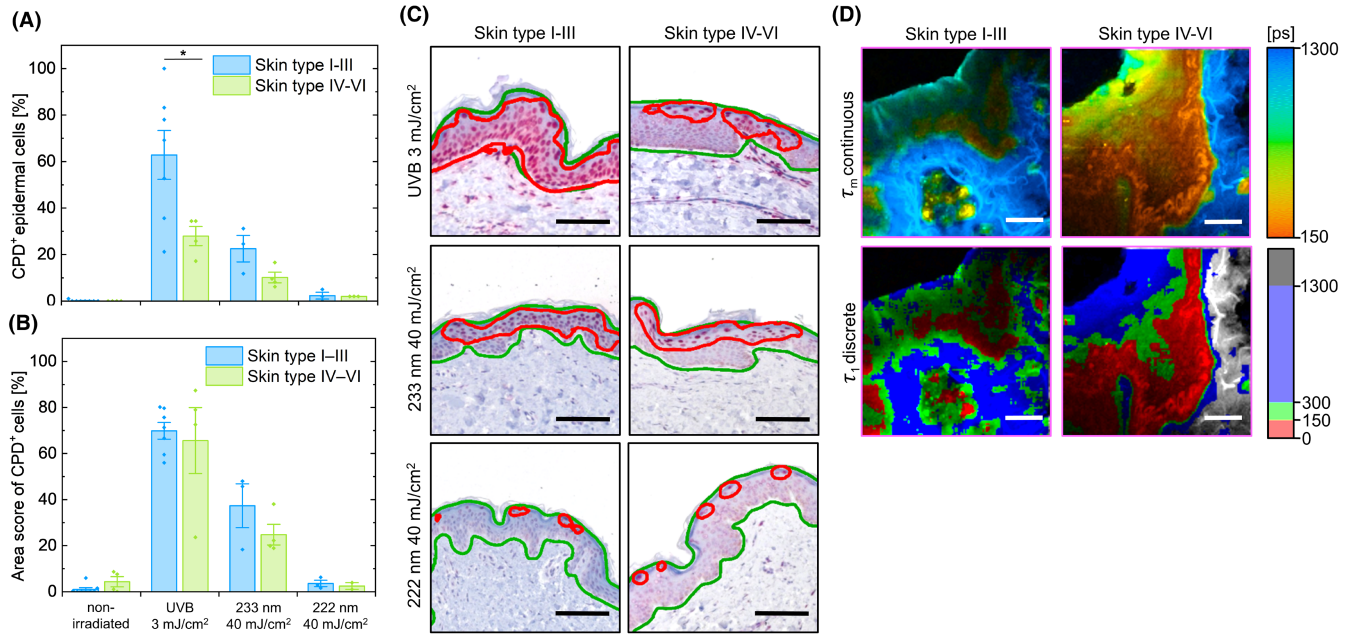

FIGURE 2 Representation of the abundance (A) as wells as area score (B) of CPD^+ epidermal cells for Fitzpatrick's skin types I–III (blue columns) and IV–VI (green columns) for irradiation with UVB 3 mJ/cm^2, 233 nm 40 mJ/cm^2 and 222 nm 40 mJ/cm^2 with corresponding representative images showing the damaged area labelled with a red line relative to the total epidermal area labelled with a green line (C). (D) shows TPE-FLIM images with the epidermal distribution of the mean fluorescence lifetime τ_m visualised continuously in false colours for lifetimes between 150 ps (orange) and 1300 ps (blue) as well as the fluorescence lifetime τ_1 shown for discrete sections in false colours with 0–150 ps (red), 150–300 ps (green) and 300–1300 ps (blue). The images show that the calculated ratio of τ_m of SG/τ_m of SB is representative for a melanin gradient in the skin. Asterisks showing statistical significance with $^*p < 0.05$ based on a two-tailed Mann–Whitney *U* test. Data of $n = 3$–7 ex vivo skin samples. Scale bars are corresponding to 100 µm (C) and 10 µm (D). The authors refer to the online version of the article for colour representation.

an indication for a photoprotective effect of melanin in the basal layer. The insignificant difference could be due to the fact that the machine learning model is not yet trained for dark skin sections and that melanin darkens the skin in the area of the basal layer even in the absence of special stains for labelling melanin, such as the Fontana-Masson stain, and can thus cause false-positive results in the machine learning model. Additionally, the depth of the epidermis is locally different in the skin, resulting in varying SG/SB thicknesses and heterogeneous photoprotective effects (Example Figure 2C). Furthermore, the intradonor distribution of melanin along the basal layer can be heterogeneous and thus lead to varying amounts of CPD^+ cells which requires the analysis of entire thin sections.

Fayujigbe et al. succeeded in visualising the differences in the degree of damage in different sections of the skin in different skin types[13,15] showing a protection of the stem cells in dark skin types, which is attributable to the photoprotective effect of melanin.[27,28] Here, fluorescence staining was used, which allows a broader range of detection of CPD^+ cells. Furthermore, it should be considered that this is a pilot study with a relatively small sample size, which was conducted ex vivo.

In the far-UVC range, differences in area were still evident for 233 nm as the damage extended to approximately the middle of the epidermis (Figure 2C), where the difference between light and dark skin types in terms of melanin content is greater than in the upper region of the epidermis (exemplary graphics of FLIM parameters τ_m and τ_1 are presented in Figure 2D). Here, the depth of DNA lesions is slightly shallower for dark skin, as compared to light skin (Figure 2C).

After irradiation with 222 nm, differences between skin types were no longer evident, although an evaluation basis was still present with 15–20 positive nuclei directly below the stratum corneum per donor evaluated.

3 | CONCLUSIONS AND PERSPECTIVES

The effects of far-UVC radiation on different skin types were evaluated for the first time in the presented pilot study. The findings give an indication that far-UVC radiation has a different effect than UVB light on different skin types. Far-UVC radiation produced less pronounced differences in DNA damage in light and dark skin types compared to UVB radiation which can be attributed to the localisation and concentration of melanin in the skin. Furthermore, it was demonstrated that differences in DNA damage between light and dark skin types might result from the different penetration depths of 222 and 233 nm far-UVC radiation. However, to confirm the hypotheses, future studies will need to look more closely at larger samples and also conduct in vivo studies. The results are important for the future application of far-UVC systems for skin decolonisation.

AUTHOR CONTRIBUTIONS

Conceptualisation: Loris Busch, Martina C. Meinke; methodology: Loris Busch, Marius Kröger, Johannes Schleusener, Silke B. Lohan, Jackie Ma; software: Marius Kröger, Jackie Ma; formal analysis: Loris Busch, Marius Kröger; investigation: Loris Busch, Marius Kröger, Daniela F. Zamudio Díaz, Johannes Schleusener, Silke B. Lohan; resources: Christian Witzel, data curation: Loris Busch, Marius Kröger, Johannes Schleusener; writing—original draft preparation: Loris Busch, Marius Kröger; writing—review and editing: Loris Busch, Marius Kröger, Daniela F. Zamudio Díaz, Johannes Schleusener, Silke B. Lohan, Jackie Ma, Christian Witzel, Cornelia M. Keck, Martina C. Meinke; visualisation, Loris Busch; supervision: Cornelia M. Keck, Martina C. Meinke; project administration: Johannes Schleusener; funding acquisition: Martina C. Meinke. All authors have read and approved the final version of the manuscript.

ACKNOWLEDGEMENTS

This work was supported by the German Federal Ministry of Education and Research (BMBF) within the projects 'VIMRE' (grant number: 03ZZ0146B) and 'CORSA' (grant number: 03COV10C). We would like to acknowledge the contributions of Heiko Gundlach, Frank Mehnke, Luca Sulmoni, Tim Wernicke, Ulrike Woggon and Michael Kneissl from Technische Universität Berlin and Hyun Kyong Cho, Thomas Filler, Johannes Glaab, Sylvia Hagedorn, Neysha Lobo Ploch, Markus Weyers, Sven Einfeldt, Ulrike Winterwerber, Lucas Wittenbecher from Ferdinand-Braun-Institut to the development of the far-UVC LED system applied in this study. We further would like to thank Anja A. Kühl and Simone Spieckermann from iPATH. Berlin-Immunopathology for Experimental Models, Charité—Universitätsmedizin Berlin for the preparation of the immunohistological sections. Furthermore, we would like to thank Maximilian Springenberg and Patrick Wagner of the Fraunhofer Heinrich Hertz Institute (HHI) for the development of the machine learning algorithm. Open Access funding enabled and organized by Projekt DEAL.

CONFLICT OF INTEREST STATEMENT

The authors state that they have no conflict of interest.

DATA AVAILABILITY STATEMENT

The data are available on reasonable request from the corresponding author.

ORCID

Loris Busch https://orcid.org/0000-0002-2671-2028
Daniela F. Zamudio Díaz https://orcid.org/0000-0002-0207-1246

REFERENCES

1. Glaab J, Lobo-Ploch N, Cho HK, et al. Skin tolerant inactivation of multiresistant pathogens using far-UVC LEDs. *Sci Rep*. 2021;11(1):14647.
2. Zwicker P, Schleusener J, Lohan SB, et al. Application of 233 nm far-UVC LEDs for eradication of MRSA and MSSA and risk assessment on skin models. *Sci Rep*. 2022;12(1):2587.
3. Narita K, Asano K, Morimoto Y, et al. Disinfection and healing effects of 222-nm UVC light on methicillin-resistant Staphylococcus aureus infection in mouse wounds. *J Photochem Photobiol B*. 2018;178:10-18.
4. Goh JC, Fisher D, Hing ECH, et al. Disinfection capabilities of a 222 nm wavelength ultraviolet lighting device: a pilot study. *J Wound Care*. 2021;30(2):96-104.
5. Buonanno M, Ponnaiya B, Welch D, et al. Germicidal efficacy and mammalian skin safety of 222-nm UV light. *Radiat Res*. 2017;187(4):483-491.
6. Ponnaiya B, Buonanno M, Welch D, Shuryak I, Randers-Pehrson G, Brenner DJ. Far-UVC light prevents MRSA infection of superficial wounds in vivo. *PloS One*. 2018;13(2):e0192053.
7. Brenner DJ. Far-UVC light at 222 nm is showing significant potential to safely and efficiently inactivate airborne pathogens in occupied indoor locations. *Photochem Photobiol*. 2023;99(3):1047-1050.
8. Eadie E, Hiwar W, Fletcher L, et al. Far-UVC (222 nm) efficiently inactivates an airborne pathogen in a room-sized chamber. *Sci Rep*. 2022;12(1):4373.
9. Buonanno M, Welch D, Shuryak I, Brenner DJ. Far-UVC light (222 nm) efficiently and safely inactivates airborne human coronaviruses. *Sci Rep*. 2020;10(1):10285.
10. Dai T, Vrahas MS, Murray CK, Hamblin MR. Ultraviolet C irradiation: an alternative antimicrobial approach to localized infections? *Expert Rev Anti Infect Ther*. 2012;10(2):185-195.
11. D'Orazio J, Jarrett S, Amaro-Ortiz A, Scott T. UV radiation and the skin. *Int J Mol Sci*. 2013;14(6):12222-12248.
12. Zamudio Díaz DF, Klein AL, Guttmann M, et al. Skin optical properties from 200–300 nm support far-UVC skin safety in vivo. *J Photochem Photobiol B, Biol*. 2023; Under Review.
13. Fajuyigbe D, Lwin SM, Diffey BL, et al. Melanin distribution in human epidermis affords localized protection against DNA photodamage and concurs with skin cancer incidence difference in extreme phototypes. *FASEB J*. 2018;32(7):3700-3706.
14. Fajuyigbe D, Young AR. The impact of skin colour on human photobiological responses. *Pigment Cell Melanoma Res*. 2016;29(6):607-618.
15. Fajuyigbe D, Douki T, van Dijk A, Sarkany RPE, Young AR. Dark cyclobutane pyrimidine dimers are formed in the epidermis of Fitzpatrick skin types I/II and VI in vivo after exposure to solar-simulated radiation. *Pigment Cell Melanoma Res*. 2021;34(3):575-584.
16. Yamaguchi Y, Takahashi K, Zmudzka BZ, et al. Human skin responses to UV radiation: pigment in the upper epidermis protects against DNA damage in the lower epidermis and facilitates apoptosis. *FASEB J*. 2006;20(9):1486-1488.
17. Del Bino S, Sok J, Bessac E, Bernerd F. Relationship between skin response to ultraviolet exposure and skin color type. *Pigment Cell Res*. 2006;19(6):606-614.
18. Kröger M, Scheffel J, Nikolaev VV, et al. In vivo non-invasive staining-free visualization of dermal mast cells in healthy, allergy and mastocytosis humans using two-photon fluorescence lifetime imaging. *Sci Rep*. 2020;10(1):14930.
19. Kröger M, Scheffel J, Shirshin EA, et al. Label-free imaging of M1 and M2 macrophage phenotypes in the human dermis in vivo using two-photon excited FLIM. *Elife*. 2022;11:e72819.
20. Pena AM, Decenciere E, Brizion S, et al. In vivo melanin 3D quantification and z-epidermal distribution by multiphoton FLIM, phasor and Pseudo-FLIM analyses. *Sci Rep*. 2022;12(1):1642.
21. Dancik Y, Favre A, Loy CJ, Zvyagin AV, Roberts MS. Use of multiphoton tomography and fluorescence lifetime imaging to investigate skin pigmentation in vivo. *J Biomed Opt*. 2013;18(2):26022.
22. Kröger M, Schleusener J, Lademann J, Meinke MC, Jung S, Darvin ME. Tattoo pigments are localized intracellularly in the epidermis and dermis of fresh and old tattoos: in vivo study using

two-photon excited fluorescence lifetime imaging. *Dermatology*. 2023;239(3):478-493.
23. Schleusener J, Lohan SB, Busch L, et al. Treatment of the Candida subspecies Candida albicans and Candida parapsilosis with two far-UVC sources to minimise mycoses in clinical practice. *Mycoses*. 2023;66(1):25-28.
24. Eadie E, Barnard IMR, Ibbotson SH, Wood K. Extreme exposure to filtered far-UVC: a case study. *Photochem Photobiol*. 2021;97(3):527-531.
25. Wagner P, Springenberg M, Kröger M, et al. Semantic modeling of cell damage prediction: a machine learning approach at human-level performance in dermatology. *Sci Rep*. 2023;13(1):8336.
26. Busch L, Kröger M, Schleusener J, et al. Evaluation of DNA lesions and radicals generated by a 233 nm far-UVC LED in ex vivo skin wounds. *J Photochem Photobiol B, Biol*. 2023; 245:112757.
27. Del Bino S, Sok J, Bernerd F. Assessment of ultraviolet-radiation-induced DNA damage within melanocytes in skin of different constitutive pigmentation. *Br J Dermatol*. 2013;168(5):1120-1123.
28. Brenner M, Hearing VJ. The protective role of melanin against UV damage in human skin. *Photochem Photobiol*. 2008;84(3):539-549.

SUPPORTING INFORMATION

Additional supporting information can be found online in the Supporting Information section at the end of this article.

Data S1. Experimental Design.

How to cite this article: Busch L, Kröger M, Zamudio Díaz DF, et al. Far-UVC- and UVB-induced DNA damage depending on skin type. *Exp Dermatol*. 2023;32:1582-1587. doi:10.1111/exd.14902